Nanoscale

ROYAL SOCIETY OF CHEMISTRY

PAPER

View Article Online
View Journal | View Issue

Cite this: *Nanoscale*, 2024, **16**, 21960

Controlling TiO_2 photocatalytic behaviour *via* perhydropolysilazane-derived SiO_2 ultrathin shell†

Darya Burak,[a,b] Jae Hyun Han,[a,c] Joon Soo Han,[a] In Soo Kim,[d,e] Md Abdur Rahman,[f] Joel K. W. Yang[f] and So-Hye Cho *[a,b]

This study addresses the inherent photocatalytic activity of pure titanium dioxide (TiO_2), which limits its application as an industrial pigment. To mitigate this issue, a core–shell structure was employed, where TiO_2 cores were encapsulated within SiO_2 shells. Perhydropolysilazane (PHPS) was introduced as a superior SiO_2 precursor over tetraethylorthosilicate (TEOS), resulting in thinner and more uniform SiO_2 shells. Utilizing TiO_2's photocatalytic properties, hydroxyl radicals facilitated the conversion of PHPS into SiO_2 *via* native Si–H bonds, eliminating the need for additional reducing agents. The formation of PHPS-derived TiO_2@SiO_2 core–shell nanoparticles demonstrated inherent self-limiting behaviour, ensuring uniform shell thickness regardless of PHPS concentration, simplifying the process for large-scale industrial applications compared to TEOS, which demands precise parameter control. Photocatalytic evaluations highlighted significant passivation of TiO_2 photocatalytic activity by PHPS-derived TiO_2@SiO_2 core–shell particles and TiO_2/SiO_2 thin films. Specifically, TiO_2@PHPS nanoparticles achieved 89–96% passivation compared to 30% with TiO_2@TEOS, while TiO_2/PHPS films degraded only 12% of Eosin B *versus* 80% with TiO_2 films. Moreover, both PHPS-derived nanoparticles and films maintained TiO_2's inherent high whiteness and high-refractive-index optical properties, underscoring their suitability for applications in white paint production, cosmetics, and high-refractive-index coatings.

Received 31st August 2024,
Accepted 4th November 2024

DOI: 10.1039/d4nr03566f

rsc.li/nanoscale

[a]*Materials Architecturing Research Centre, Korea Institute of Science and Technology, 5 Hwarang-ro 14-gil, Seoul 02792, Republic of Korea. E-mail: sohyec@kist.re.kr*
[b]*Division of Nano & Information Technology, University of Science and Technology, 217 Gajeong-ro, Yuseong-gu, Daejeon 34113, Republic of Korea*
[c]*Display and Nanosystem Laboratory, College of Engineering, Korea University, Anam-ro 145, Seoul 02841, Republic of Korea*
[d]*Nanophotonics Research Centre, Korea Institute of Science and Technology, 5 Hwarang-ro 14-gil, Seoul 02792, Republic of Korea*
[e]*KIST-SKKU Carbon-Neutral Research Centre, Sungkyunkwan University (SKKU), 25-2 Seonggyungwan-ro, Suwon 16419, Republic of Korea*
[f]*Division of Engineering Product Development, Singapore University of Technology and Design, 8 Somapah Road, Singapore 487372, Singapore*

† Electronic supplementary information (ESI) available: Camera-captured images of PHPS solution after UV-C and UV-A irradiation (Fig. S1), HRTEM images of TiO_2@PHPS nanoparticles prepared under UV-A-irradiated and non-irradiated conditions (Fig. S2), impact of UV-A irradiation time on formation of PHPS-derived SiO_2 shell: XRD (Fig. S3), SAED patterns (Fig. S4), FT-IR spectra (Fig. S5), TEM (Fig. S6) and HRTEM (Fig. S7) images, photocatalytic degradation graph (Fig. S8) of Eosin B by TiO_2, TiO_2@TEOS, and TiO_2@PHPS nanoparticles, where TiO_2@PHPS nan-particles were synthesized under 1, 3, and 5 h UV-A irradiation, deconvoluted C1s XPS spectrum of TiO_2@TEOS nanoparticles (Fig. S9), TEM images of ZnO@PHPS and TiO_2 rutile@PHPS nanoparticles prepared *via* self-catalyzed method (Fig. S10), colour characterization table of TiO_2, TiO_2@TEOS and TiO_2@PHPS nanoparticles (Table S1), as well as TiO_2 and TiO_2/PHPS films (Table S2), GIXRD patterns (Fig. S11), ellipsometry-measured refractive indices (Fig. S12), pencil hardness and cross-cut adhesion test results (Table S3), camera-captured and microscopic images of TiO_2 and TiO_2/PHPS films after pencil hardness (Fig. S13) and cross-cut adhesion (Fig. S14) tests. See DOI: https://doi.org/10.1039/d4nr03566f

Introduction

TiO_2 nanoparticles have gained significant attention due to their exceptional chemical stability, optical properties, and photocatalytic activity.[1–3] TiO_2 widespread applications in various industries, including paints,[4] plastics,[5] cosmetics,[6] foods,[7] solar cells, and high-refractive-index coatings,[8] attest to their versatility. For instance, TiO_2 finds use as a UV absorber[9] in sunscreens, foundations, and other makeup products, where it acts as a physical barrier that reflects and scatters UV radiation away from the skin. In white paint production, especially for applications such as car exteriors, the use of TiO_2 as a coating is also crucial due to its high refractive index ($n \geq 2.4$).[10] Nevertheless, the unrestricted production of free radicals when TiO_2 is exposed to UV radiation inadvertently raises concerns.[11,12] As a photocatalytic material, TiO_2 generates highly reactive radicals, such as $^{\bullet}OH$ and $^{\bullet}O_2^-$, which can deteriorate organic pigment coatings and cause skin irritation,[13] highlighting the need to control and passivate its photocatalytic activity.

To control photocatalytic activity of TiO_2 while maximizing its refractive characteristics, a thin shielding shell is essential. While too thin shells (<1.4 nm) cannot be effective and rather enhance TiO_2 photocatalytic properties,[14] overly thick shells could lower the overall refractive index, rendering TiO_2 high-

refractive-index properties ineffective. Hence, it is essential to achieve an optimal balance in shell thickness to preserve both the desired refractive characteristics and effective passivation of TiO_2 photocatalytic activity.

Traditionally, a barrier shell is applied to the TiO_2 core to passivate its photocatalytic activity, and silica is the predominant shielding material due to its cost-effectiveness and facile fabrication methods.[15–19] One of the most commonly used methods, the Stöber method,[20–22] is renowned for producing SiO_2 nanoparticles from TEOS (tetraethylorthosilicate). Nevertheless, the Stöber method is associated with a slow reaction rate requiring prolonged reaction times. Furthermore, it has been reported that SiO_2 shells synthesized from TEOS must be sufficiently thick to effectively passivate the TiO_2 photocatalytic activity, owing to the microporosity inherent to TEOS-derived SiO_2 shells caused by ethanol used as the solvent.[16,23,24] As mentioned above, a thick silica shell can lead to a reduction in the overall refractive index of TiO_2, which, in turn, diminishes its high-refractive-index properties essential for commercial applications.

To address the challenges associated with achieving effective passivation of TiO_2 photocatalytic activity while using a thinner silica coating, we fabricated TiO_2@SiO_2 core–shell particles using PHPS (perhydropolysilazane) as an alternative to TEOS. PHPS, an inorganic polymer containing Si–N, Si–H, and N–H bonds, undergoes a transformation into silica when exposed to atmospheric moisture at relatively low temperatures (<200 °C).[25–27] Compared to TEOS, PHPS offers coatings of higher density,[28] reduced crack formation, and lower porosity. Despite these advantages, PHPS has been far less frequently reported as a silica shell precursor in literature.

Our method utilizes the photocatalytic properties of TiO_2 under UV light to convert PHPS into silica *via* hydroxyl radicals inherent to TiO_2, achieving enhanced control over SiO_2 agglomeration and allowing the deposition of a thinner, uniform silica shell on the TiO_2 core. This improved process resulted in effective photocatalytic passivation by the PHPS-derived TiO_2@SiO_2 core–shell particles and SiO_2/TiO_2 thin films, as demonstrated through photocatalytic degradation reactions with Eosin B. Colourimetric measurements showed that the high-refractive-index and whiteness of TiO_2 were not affected by the silica coating. Consequently, this approach offers superior photocatalytic passivation and UV protection, making it suitable for cosmetics and paints, and applicable in high-refractive-index optical coatings for lenses and mirrors.

Experimental

Materials

Titanium dioxide (TiO_2) powder was prepared from the commercial TiO_2 P25 powder (nanoparticle mean size ~20 nm) purchased from Sigma Aldrich (Darmstadt, Germany). ZnO nanoparticles (NPs) were synthesized *via* light-assisted sulfidation of ZnO NPs.[29] Rutile TiO_2 was purchased from Junsei Chemical Co. Ltd (Tokyo, Japan). Perhydropolysilazane (PHPS) (Product Number: CISD-15001, 18.6 wt% in dibutyl ether) was sourced from Samsung SDI (Yongin-si, South Korea). Tetraethylorthosilicate (TEOS) and Eosin B were purchased from Alfa Aesar (Ward Hill, MA, USA). Dibutyl ether (DBE), ethyl alcohol (EtOH, 95%), and isopropyl alcohol (IPA, 99.5%) were obtained from Daejung Chemicals & Metals Co. Ltd (Daejung, South Korea). Aqueous ammonia solution (28 wt% NH4OH) and titanium butoxide (TBOT, 97%) were purchased from Junsei Chemical Co. Ltd (Tokyo, Japan) and Sigma Aldrich (Darmstadt, Germany), respectively. These compounds were used as received without further purification. Deionized water (DI, 14.6 MΩ cm, Millipore Milli-Q lab water system) was used throughout all experiments.

Fabrication of TiO_2@SiO_2 core–shell nanoparticles

To prepare the PHPS-derived TiO_2@SiO_2 nanoparticles, 200 mg of TiO_2 P25 powder was homogeneously dispersed in 20 ml of DBE by sonication for 30 min. Then, the solution was stirred vigorously under UV-A irradiation (365 nm) for 1 h to activate the TiO_2 nanoparticles. Subsequently, a PHPS solution (0.5, 1, and 2 ml) was injected into the TiO_2 nanoparticles solution, and the mixture was sonicated in a water bath under UV-A irradiation for 1, 3 and 5 h. The resulting nanoparticles were separated from the solution *via* centrifugation (10 000 rpm, 15 min) and washed 3 times with DBE. The particles were then dried in a vacuum oven at 150 °C for 3 h. Throughout the subsequent text, the samples synthesized with PHPS will be referred to as TiO_2@PHPS and PHPS-derived TiO_2@SiO_2 core–shell nanoparticles.

In a control experiment, PHPS alone was exposed to UV light. Under UV-C irradiation (254 nm), PHPS showed an increase in haze level, indicating silica formation, confirming that PHPS absorbs UV-C light. However, under UV-A light, PHPS showed no reaction, signifying no transformation into silica. This indicated that silica formation under UV-A light results from the activation of TiO_2, highlighting the self-catalysed coating phenomenon of TiO_2 particles in converting PHPS to SiO_2 (Fig. S1†).

For the synthesis of the TEOS-derived TiO_2@SiO_2 nanoparticles, 100 mg of TiO_2 P25 powder was homogeneously dispersed in 140 ml of EtOH by sonication for 30 min. Then, a TEOS solution (0.7, 1, and 1.4 ml) containing 9 ml of DI water and 3 ml of NH_4OH (added dropwise) was injected in the TiO_2 nanoparticles solution and stirred vigorously for 2 h. The resulting core–shell nanoparticles were separated from the solution by centrifugation (10 000 rpm, 15 min) and washed 3 times with ethanol. The particles were then dried in a vacuum oven at 80 °C for 3 h. Throughout the subsequent text, the samples synthesized with TEOS will be referred to as TiO_2@TEOS and TEOS-derived TiO_2@SiO_2 core–shell nanoparticles.

Fabrication of PHPS-derived SiO_2/TiO_2 thin films

The PHPS-derived SiO_2/TiO_2 films were fabricated on Si wafer substrates. The substrates were ultrasonically cleaned in EtOH, IPA, and DI water, followed by drying under a stream of argon.

Further elimination of surface contaminants was achieved through UV/ozone cleaning using a UV Ozone Cleaner UVC-30S (Jaesung Engineering Co., South Korea).

TiO_2 films were deposited on the Si wafer substrates *via* spin-coating at 3000 rpm for 30 s. TBOT was used as a precursor and was dissolved in EtOH in a 1 : 7 ratio. Subsequently, the TBOT-deposited films were dried on a hot plate at 300 °C for 30 min to remove any residual EtOH solvent and initiate the hydrolysis process, resulting in evaporation of butoxide groups and formation of amorphous TiO_2 films. The amorphous films were then crystallized to anatase TiO_2 by annealing in a furnace at 500 °C for 15 min.

To subsequently deposit a PHPS-derived SiO_2 film, the PHPS precursor solution was first dissolved in DBE in a 1 : 4 ratio. The TiO_2 film was then placed at the bottom of a Petri dish, and the prepared PHPS solution was poured over it to ensure complete coverage. The reaction system was then exposed to UV-A irradiation for 10 min. After the deposition, the PHPS-derived films were dried on a hot plate at 200 °C for 1 h. Throughout the subsequent text, these samples will be referred to as TiO_2/PHPS films.

Photocatalytic activity investigation

The photocatalytic activity of the TiO_2@SiO_2 core–shell particles was evaluated through the photodegradation of Eosin B. A 10 mg sample was dispersed in 20 ml of Eosin B solution (4.5×10^{-6} mol L^{-1}), kept in darkness for adsorption–desorption equilibrium and irradiated with a 365 nm UV-A lamp (Sankyodenki, Japan) for 5 to 7 h. Absorbance at 517 nm was measured to determine degradation using a calibration curve. For TiO_2/SiO_2 thin films, 2 ml of Eosin B solution was applied to 2.5 × 2.5 cm samples, irradiated for 3 h, and the absorbance was measured similarly.

Characterization

The composition analysis of the TiO_2@TEOS and TiO_2@PHPS core–shell nanoparticles was carried out using Fourier-transform infrared (FT-IR) spectroscopy with a scan range of 4000–400 cm^{-1} in reflectance mode (Bruker ALPHA II Compact FT-IR Spectrophotometer, USA). Morphology of the core–shell nanoparticles and cross-section morphology of the TiO_2/SiO_2 thin films were examined by transmission electron microscopy (TEM) (FEI Tecnai F20 G2, USA). Cross-section samples were prepared utilizing the focused-ion-beam (FIB) technique. Composition and bonding states in the TiO_2@SiO_2 core–shell particles were determined *via* X-ray photoelectron spectroscopy (XPS) (Nexsa photoelectron spectrometer, Thermo Fisher Scientific, USA). The phases of SiO_2 and TiO_2 were identified through X-ray diffraction (XRD) analysis (Bruker DE/D8 Advance, USA).

In photocatalytic activity experiments, the concentration of Eosin B solutions was determined from UV-vis absorption spectra using a UV-vis spectrophotometer (Varian Cary100, Agilent Technologies, USA). The whiteness and high-refractive-index properties of the TiO_2@SiO_2 nanoparticles and TiO_2/SiO_2 thin films were assessed through colourimetric measurements. Reflectance spectra were measured with a spectrophotometer (Konica Minolta CM 3600A, Japan) equipped with a white xenon light source with a 4 mm diameter beam. Colour parameters were derived using Spectra-Magic NX Colour Data Software (Konica Minolta)[30] and represented in the CIELAB ($L^*a^*b^*$) colour space, where L^* is brightness, and a^* and b^* are primary colours of human vision (red, green, blue, and yellow). Additionally, reflectance spectra of the TiO_2/PHPS thin films were simulated for comparison with measured data. The films' refractive indices were determined *via* ellipsometry measurements and employed to simulate the reflectance spectra and colours. This simulation involved the modulation of multilayered thin films with known thicknesses and reflective indices of the TiO_2 and SiO_2 layers, using the characteristic matrix calculation in the OpenFilters Software.[31]

Results and discussion

TiO_2@SiO_2 core–shell nanoparticles synthesis by passive (TEOS) and self-catalyzed (PHPS) methods

In this study, TiO_2@SiO_2 core–shell nanoparticles were synthesized *via* two different methods to assess their efficacy in passivating the photocatalytic activity of TiO_2. Fig. 1 illustrates the formation process of the TiO_2@TEOS and TiO_2@PHPS nanoparticles. The synthesis method employing TEOS, referred to as the 'passive method', was adapted from the Stöber method detailed in prior literature.[20–22] By this method, silica shells are formed through the hydrolysis and condensation of TEOS mixed with water and NH_4OH in an EtOH solution, with NH_4OH serving as a catalyst.

By another method proposed in our study, 'self-catalysed method', SiO_2 shells are synthesized from PHPS, making advantageous use of the intrinsic TiO_2 photocatalytic properties. The abundant Si–H groups in PHPS[32] render it highly reactive with hydroxyl radicals formed on the surface of TiO_2 by irradiation with UV light. The generated radicals catalyse PHPS hydrolysis, leading to the formation of short-lived silanol groups. Ultimately, condensation and cross-linking reactions result in the formation of a silica shell.

When TiO_2 is activated under UV light, hydroxyl radicals are generated around the TiO_2 core,[33] and silica formation proceeds uniformly around it. Thus, this process can prevent SiO_2 aggregation and provide ultrathin uniform shells. To validate this, Fig. S2† shows HRTEM images of TiO_2@PHPS nanoparticles prepared under both UV-irradiated (1, 3, and 5 h irradiation) and non-irradiated conditions. In non-irradiated samples, the shell state was not smooth, along with observed aggregation phenomena. On the other hand, in the irradiated samples, where TiO_2 particles were activated under UV-A light (365 nm), the hydroxyl radicals generated *via* photocatalysis facilitated better adherence of silica particles to the TiO_2 core, resulting in a smooth and uniform shell without any aggregation.

Additionally, we conducted preliminary experiments to determine the optimal duration of UV-A light irradiation

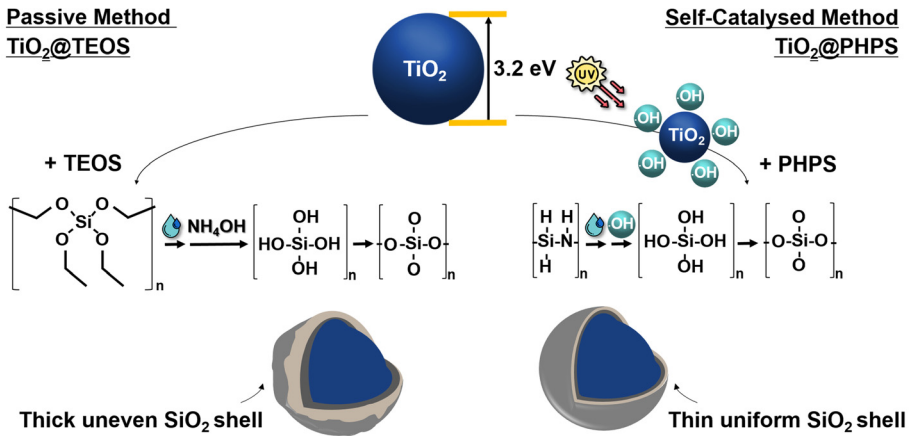

Fig. 1 Schematic representation of the TiO_2@TEOS core–shell nanoparticles prepared *via* 'passive method', and the TiO_2@PHPS core–shell nanoparticles prepared *via* 'self-catalysed method'.

required for the complete formation of the PHPS-derived SiO_2 shell. The irradiation time was varied from 1, 3 to 5 h. It was determined that an irradiation time of 3 h was optimal for sufficient conversion of PHPS into SiO_2 and formation of a uniform thin film. Detailed description of this experiment is provided in the ESI (Fig. S3–S8†).

The XPS analysis was conducted to assess the structure of the 0.7 mL TiO_2@TEOS and 1 mL 3 h irradiated TiO_2@PHPS core–shell nanoparticles with similar thicknesses (2 nm) by examining peaks of interest, namely O 1s, Ti 2p, Si 2p, and C 1s (Fig. 2). For the uncoated TiO_2 particles, the O 1s spectrum (Fig. 2b) exhibited two discernible peaks at binding energies of 531.5 and 529.6 eV, corresponding to absorbed water molecules and O_2^- ions within the TiO_2 lattice (Ti–O), respectively.[34,35] Conversely in the TiO_2@PHPS nanoparticles, the O 1s deconvoluted spectrum displayed three peaks at 533.5, 532.7, and 530.0 eV, while in the TiO_2@TEOS nanoparticles, these peaks appeared at 533.2, 532.6, and 530.0 eV. The peak at 530.0 eV indicated O_2^- ions within the TiO_2 lattice (Ti–O),[35,36] while peaks at 532.7/532.6 eV were associated with the O_2^- in the SiO_2 lattice. The peaks at 533.5/533.2 eV were attributed to the Si–OH groups and adsorbed water.[14,35,36] The shift from 529.6 eV to 530.0 eV of the Ti–O bond suggested successful deposition of SiO_2 onto TiO_2, forming Ti–O–Si bonds.[14,37,38] Furthermore, a significant decrease in the intensity of the Ti–O bond in the TiO_2@PHPS and TiO_2@TEOS nanoparticles supported the evidence that the SiO_2 shell successfully formed on the surface of TiO_2.[36]

For the Ti 2p peak (Fig. 2c), the uncoated TiO_2 nanoparticles exhibited two peaks at 458.4 and 464.1 eV, corresponding to Ti^{4+} $2p_{3/2}$ and Ti^{4+} $2p_{1/2}$, respectively.[35,39] In contrast, both TiO_2@PHPS and TiO_2@TEOS nanoparticles showed shifted peaks at 458.6 and 464.4 eV, and 458.5 and 464.3 eV, indicating an increase in binding energy of the Ti 2p inner shell electrons due to the SiO_2 shell, affirming the Ti–O–Si bond formation. The reduction in electron density near the Ti atom resulted from the higher electronegativity of Si interacting with O around the Ti atom. This, in turn, weakened the shielding effect, leading to an increase in the binding energy of the TiO_2@SiO_2 core–shell nanoparticles.[36] Furthermore, it was observed that the peaks of the TiO_2@PHPS nanoparticles shifted slightly more than those of the TiO_2@TEOS nanoparticles. This difference suggests a stronger Ti–O–Si bond in the TiO_2@PHPS nanoparticles, likely due to hydroxyl radicals inducing the formation of the SiO_2 nanoparticles directly on the surface of TiO_2 nanoparticle core. Conversely, in the case of TEOS, the formation is passive, where the adherence was primarily due to a weaker interaction between the TiO_2 core and the SiO_2 nanoparticles. Valence-band XPS (VB XPS) analysis of the TiO_2, TiO_2/TEOS, and TiO_2/PHPS films further confirmed the formation of the Ti–O–Si bond.[40] As shown in Fig. S9a,† the valence band maximum of the TiO_2/PHPS film shifted to 3.6 eV after SiO_2 layer formation, from 2.1 eV for the TiO_2 film, while no significant shift was observed for the TiO_2/PHPS film. This reinforces that the 'self-catalysed method' yields stronger Ti–O–Si bonding.

The sharp peak at 103.4 eV in the Si 2p spectrum (Fig. 2d) of the TiO_2@PHPS nanoparticles confirmed the presence of SiO_2 on the TiO_2 surface.[41] However, in the case of the TiO_2@TEOS nanoparticles, the peak appeared broader and slightly shifted, prompting a detailed analysis of the spectrum. In the TiO_2@TEOS nanoparticles, the Si 2p spectrum revealed two distinct peaks at 103.4 and 102.5 eV, corresponding to SiO_2 and SiO_x–C, respectively.[42] This led to the conclusion that in the case of the TEOS-derived TiO_2@SiO_2 nanoparticles, carbon was still present due to the organic origin of TEOS. This was further supported by studying the C 1s peak of the TiO_2@TEOS nanoparticles.

For the TiO_2@TEOS nanoparticles, the full scan survey XPS spectrum (Fig. 2a) demonstrated a significantly high peak of C 1s, indicating a substantial carbon component remaining from the organic origin of TEOS after its conversion into SiO_2 during the nanoparticle fabrication process. The presence of these carbon components (Fig. S9b†) in the TiO_2@TEOS nano-

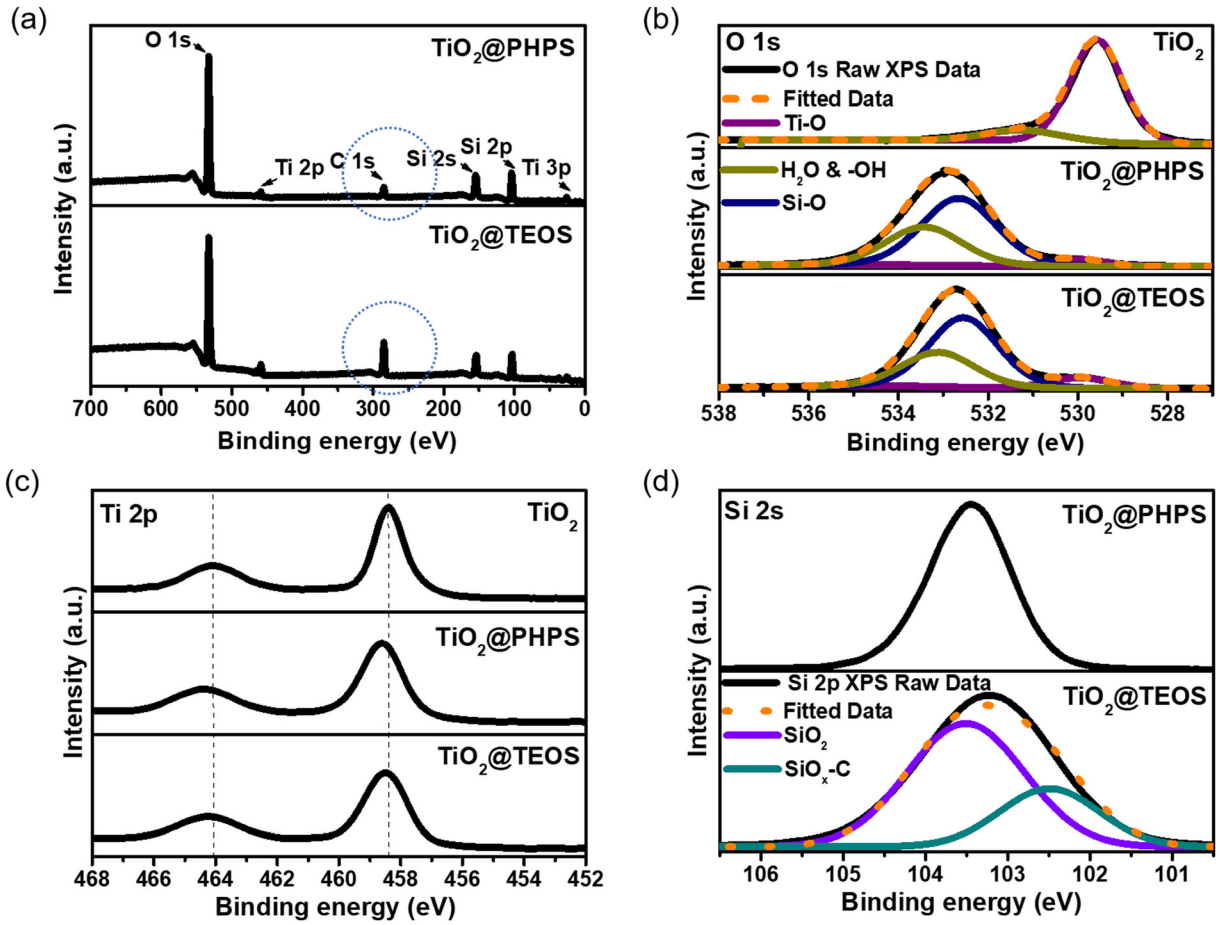

Fig. 2 (a) Full scan survey XPS spectra of 0.7 mL TiO_2@TEOS and 1 mL 3 h irradiated TiO_2@PHPS core–shell nanoparticles. Narrow-scan XPS spectra of (b) deconvoluted O 1s, (c) Ti 2p, and (d) deconvoluted Si 2p binding energy ranges of the TiO_2, TiO_2@TEOS, and TiO_2@PHPS core–shell nanoparticles.

particles was speculated to affect the purity and whiteness of the nanoparticles. In the case of TiO_2@PHPS nanoparticles, small peak of C1s was likely due to hydrocarbon impurities during solvent contamination.

Self-catalysed method: effect of precursor concentration on SiO_2 shell thickness

Since the irradiation time of 3 h was determined to be optimal for sufficient conversion of PHPS into SiO_2 as detailed in the previous section, the irradiation time was maintained at 3 h for all TiO_2@PHPS nanoparticles in this experiment. In this experiment, we aimed to demonstrate that the self-catalysed formation of the TiO_2@PHPS nanoparticles is an inherently self-limiting process. This means that irrespective of the PHPS pre-cursor concentration, only a fixed amount of PHPS can interact with the hydroxyl radicals on the TiO_2 surface. Consequently, any excess PHPS remains unreacted and is removed from the system. This self-limiting behaviour leads to the formation of uniform shells with a constant thickness of the TiO_2@PHPS nanoparticles. In contrast, the shell thickness of TiO_2@TEOS nanoparticles is highly dependent and varies with the concentration of the TEOS precursor.

As can be inferred from FT-IR measurements presented in Fig. 3a, the intensity of the Si–O–Si bond has undergone a substantial increase with the increase in TEOS concentration. Thus, it was confirmed that the TEOS-derived SiO_2 shells are typically greatly influenced by the concentration of TEOS (Fig. 3b), necessitating tedious control over the experimental parameters. On the other hand, FT-IR spectra of the TiO_2@PHPS nanoparticles revealed no change in the intensity of the Si–O–Si bond with different PHPS concentrations (Fig. 3c), suggesting that the thickness of the SiO_2 shell did not undergo any substantial changes. The following suggests that a certain amount of PHPS can come into contact with hydroxyl radicals of TiO_2, thus meaning that the excess amount of PHPS would stay unreacted and discarded from the system after the reaction. The following postulation was supported by the HRTEM measurements presented in Fig. 3d and Fig. S10,† whereupon the thickness of the TiO_2@PHPS nanoparticles remained at 2 nm regardless of the PHPS concentration variation.

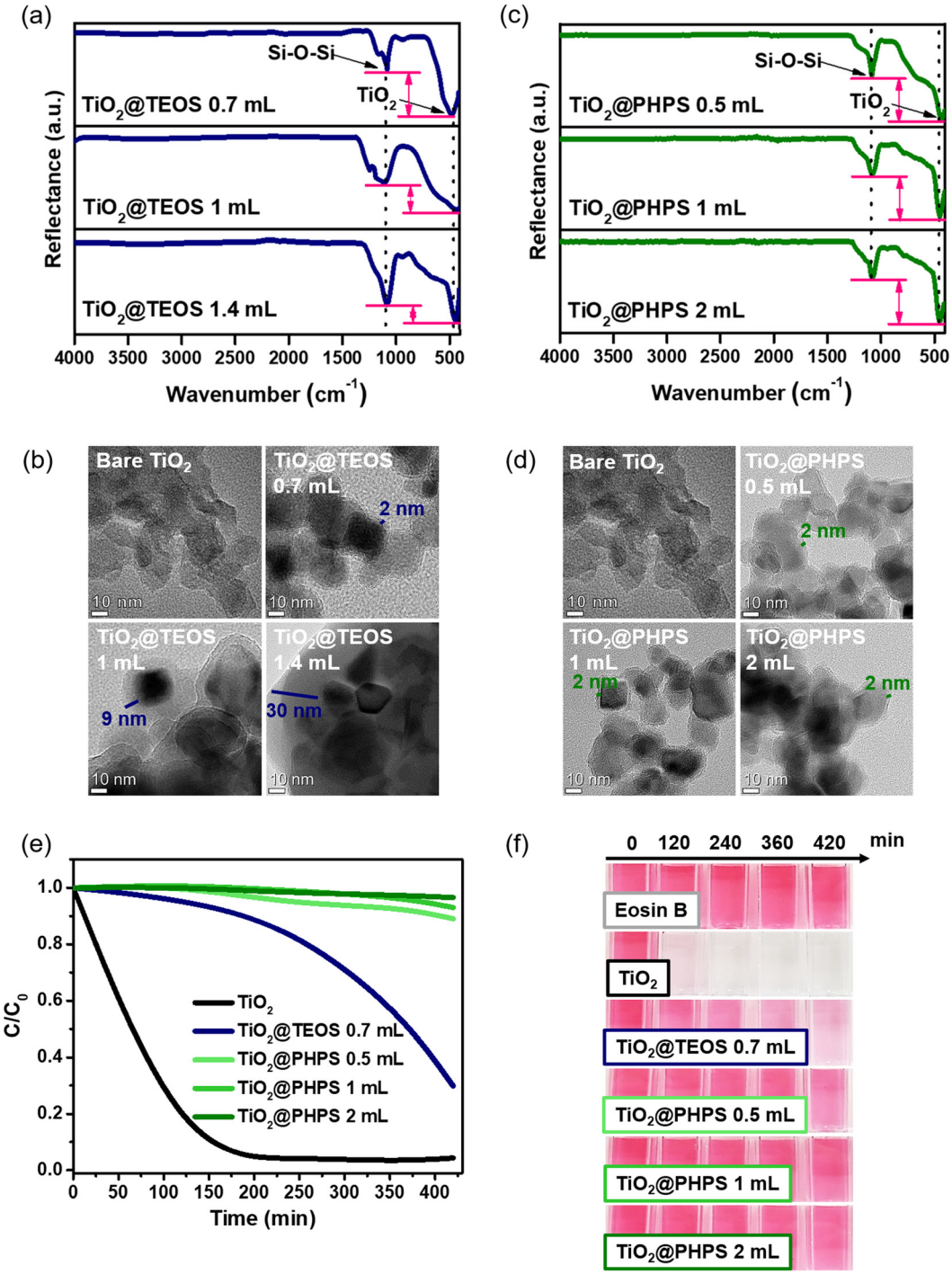

Fig. 3 FT-IR spectra of the (a) 0.7, 1, and 1.4 mL TiO_2@TEOS and (c) 0.5, 1, and 2 mL TiO_2@PHPS core–shell nanoparticles. HRTEM images of the (b) TiO_2, 0.7, 1, and 1.4 mL TiO_2@TEOS and (d) 0.5, 1, and 2 mL TiO_2@PHPS core–shell nanoparticles. (e) Photocatalytic degradation of Eosin B as a function of time by the TiO_2, 0.7 mL TiO_2@TEOS and 0.5, 1 and 2 mL TiO_2@PHPS core–shell nanoparticles. (f) Camera-captured images of the Eosin B solution following its photocatalytic degradation by the TiO_2, TiO_2@TEOS and TiO_2@PHPS core–shell nanoparticles under UV-A irradiation (365 nm).

The PHPS-derived TiO_2@SiO_2 nanoparticles, prepared using varying concentrations of PHPS, demonstrated comparable passivation abilities of photocatalytic TiO_2, reaching as high as 89–96% passivation observed after 420 min of Eosin B photodegradation reaction (Fig. 3e and f). Moreover, all PHPS-derived nanoparticles exhibited superior passivation performance compared to those derived from TEOS (0.7 mL, 2 nm thickness), which only reached 30% passivation.

For proof-of-concept, we have also demonstrated that other photocatalytic materials can be used in the self-catalysed method to successfully fabricate a SiO_2 shell. Fig. S11a† demonstrates the uniform SiO_2 shell on the ZnO nanoparticle core by reacting photocatalytic ZnO and PHPS. The self-catalysed method was effective because ZnO exhibits photocatalytic activity under UV-A irradiation. On the other hand, we have also demonstrated that this method will not be applicable to rutile TiO_2 since the photocatalytic activity of rutile under UV-A irradiation is generally known to be weaker com-pared to anatase.[43,44] Hence, the self-catalysed coating was not dominant, and, as can be observed from TEM images in Fig. S11b,† SiO_2 particles aggregated segmentally on the surface of the TiO_2 core.

Whiteness assessment of TiO_2@PHPS core–shell nanoparticles

In order to assess the practical suitability of the TiO_2@PHPS core–shell nanoparticles for the white paint production, the colourimetric properties of the fabricated nanoparticles were analysed. According to the Hunter Whiteness Formula,[45] a higher value of L^* (lightness) indicates greater whiteness in the sample. Additionally, the closer the values of a^*b^* parameters are to 0, the whiter the sample appears.

Analysis of the CIELAB a^*b^* diagram depicted in Fig. 4 revealed that a^*b^* parameters of the TiO_2@PHPS nanoparticles were generally closer to those of bare TiO_2. This suggested superior preservation of whiteness parameters in the TiO_2@PHPS nanoparticles compared to TiO_2@TEOS, where the a^*b^* parameters were more widely scattered on the diagram. Further insights from Table S1† indicated that the TiO_2@PHPS nanoparticles exhibited higher whiteness than the TiO_2@TEOS nanoparticles when comparing their $L^*a^*b^*$ parameters. On the other hand, the whiteness of the TiO_2@TEOS nanoparticles was speculated (as elaborated in the XPS analysis description above) to be affected by carbon impurities.

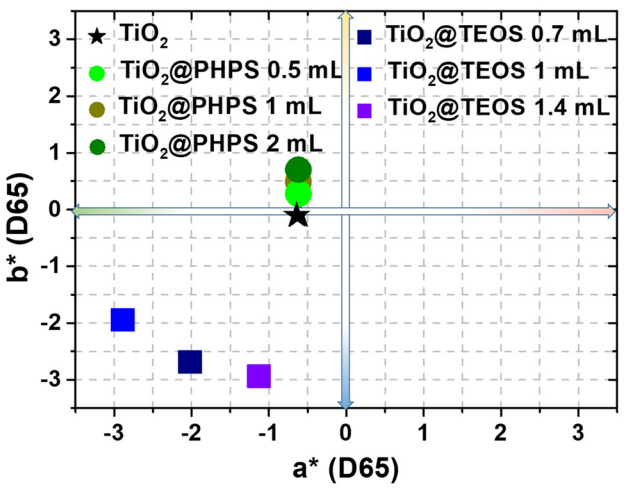

Fig. 4 CIE a^*b^* chromaticity diagram of whiteness parameters of the TiO_2, TiO_2@TEOS, and TiO_2@PHPS core–shell nanoparticles fabricated in this study with different TEOS and PHPS precursor concentrations.

Application of the PHPS-derived SiO_2 coating on high-refractive-index TiO_2 thin film

Building upon the remarkable passivation of photocatalytic activity observed in the TiO_2@PHPS core–shell nanoparticles, we extended this concept to thin films to explore how the PHPS-derived SiO_2 films deposited on TiO_2 would passivate its photocatalytic ability (Fig. 5a).

While no humps indicative of an amorphous SiO_2 layer were observed in XRD measurements (Fig. S12†), cross-sectional analysis of the PHPS-derived TiO_2/SiO_2 film revealed the presence of SiO_2 (Fig. 5b). A clearly defined top SiO_2 layer was deposited on the surface of the TiO_2 layer. Since the PHPS-derived SiO_2 layer fully covered the TiO_2 surface, it was expected to exhibit superior passivation of the TiO_2 photocatalytic activity.

Following this hypothesis, photocatalytic experiments were conducted, and the results are presented in Fig. 5c and d. Fig. 5c shows that the concentration of Eosin B exhibited rapid decay for the bare TiO_2 film, reaching an 80% degradation after 180 min of UV-A irradiation. In contrast, the TiO_2/PHPS film showed no significant decrease in Eosin B concentration until 120 min, after which it began to exhibit gradual decay, showing only a 12% decrease (88% passivation) after 180 min of irradiation.

Next, to investigate how the introduction of the PHPS-derived SiO_2 layer affected the inherent high-refractive-index optical properties of the TiO_2 film, the optical performance of the TiO_2/PHPS film was studied. The refractive indices of the films were measured *via* ellipsometry (Fig. S13,† n = 2.4 at 550 nm), and the reflectance spectra were simulated for the comparison with the measured counterparts. The TiO_2/PHPS film was considered as a two-layer structure with the independent TiO_2 and PHPS-derived SiO_2 layers of 82.1 and 9.8 nm thickness values, respectively. Fig. 6a and b displays the measured and simulated reflectance spectra of the films. The simulated reflectance spectra aligned well with the measured counterparts.

In the case the TiO_2/PHPS film, a slight redshift in the reflectance spectra was observed following the introduction of SiO_2 onto the TiO_2 film. This redshift occurred due to the increased number of layers, leading to an overall increase in film thickness and constructive interference. However, since the thickness of the SiO_2 layer in the film was relatively small, only 9.8 nm, it had a minor impact on the interference pattern, resulting in a subtle redshift.[46,47] Thus, the introduction of PHPS-derived SiO_2 layer had a negligible effect on the intrinsic optical properties of the TiO_2 layer, without significantly influencing the colour and high-refractive-index properties of the initial TiO_2 film, while successfully passivating TiO_2 photocatalytic activity.

From the CIE a^*b^* chromaticity diagram depicted in Fig. 6c, it was further demonstrated that the colour of the TiO_2/PHPS film closely resembled that of the initial TiO_2 film in terms of the a^*b^* colour parameters. Table S2† presents the measured colours and their respective colourimetric parameters.

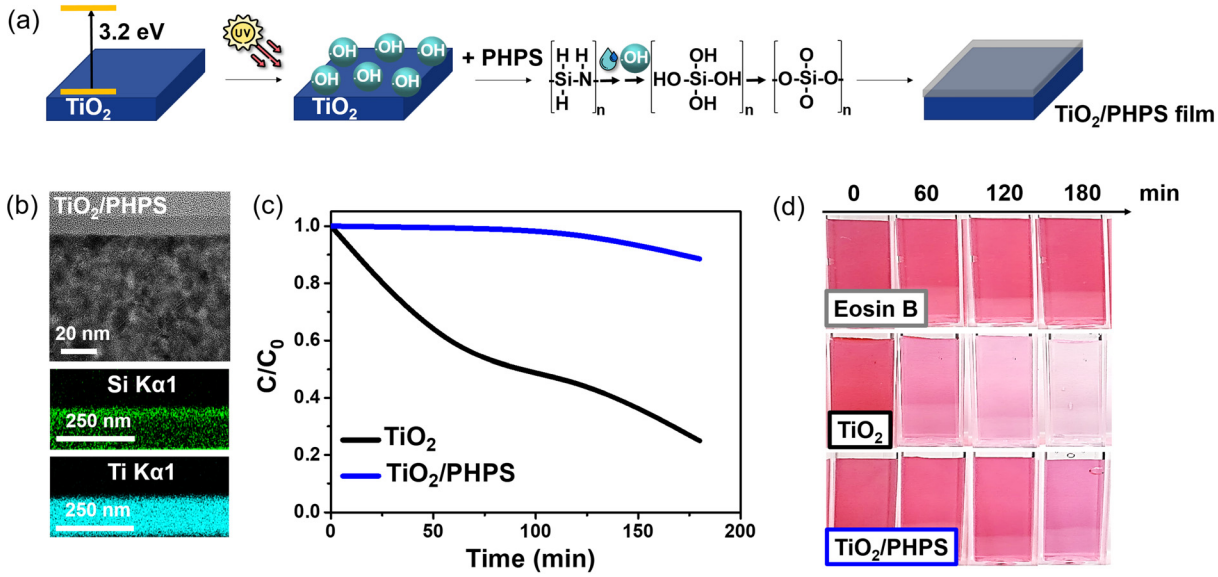

Fig. 5 (a) Schematic representation of the TiO_2/PHPS film prepared *via* 'self-catalysed method'. (b) Cross-sectional TEM images of the TiO_2/PHPS thin film. (c) Photocatalytic degradation of Eosin B as a function of time by the TiO_2 and TiO_2/PHPS thin films. (d) Camera-captured images of the Eosin B solution following its photocatalytic degradation by the TiO_2 and TiO_2/PHPS films under UV-A irradiation.

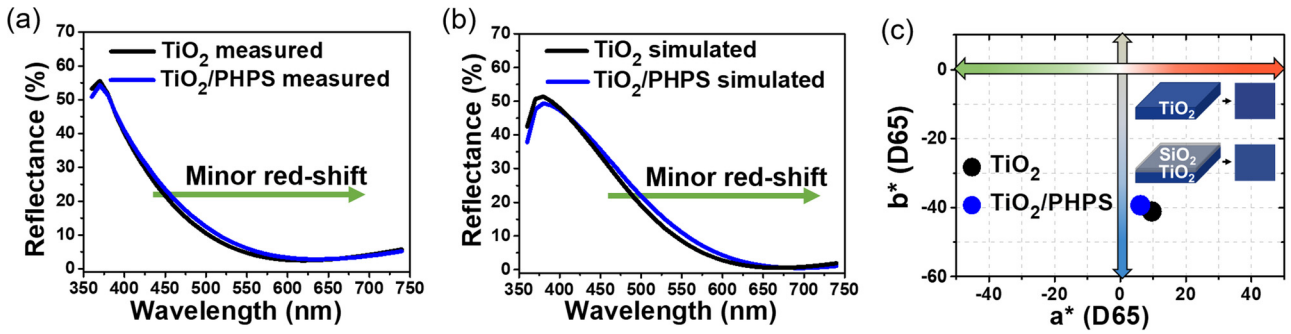

Fig. 6 (a) Measured and (b) simulated reflectance spectra of TiO_2 and TiO_2/PHPS films. (c) CIE *a*b** chromaticity diagram of colour parameters of the TiO_2 and TiO_2/PHPS films. Insert in top right corner illustrates measured colours and their corresponding films.

Lastly, the TiO_2 and TiO_2/PHPS films were subjected to standardized wear resistance tests to assess their suitability for practical applications, with results depicted in Table S3.† Fig. S14† demonstrated that the hardness of the TiO_2 and TiO_2/PHPS films reached 4H, close to the reported value of 5H for sol–gel-derived SiO_2/TiO_2 coatings.[48] Adhesion was also evaluated using tapes with varying adhesion strengths, with attachment/detachment performed up to 10 times (Fig. S15†). Microscopic examination after the cross-cut test revealed no visible delamination or fragment separation, indicating strong adhesion of both TiO_2 and SiO_2/TiO_2 films.

Conclusions

This study introduced a novel method using perhydropolysilazane (PHPS) to create an ultrathin uniform silica shell on TiO_2 *via* a self-catalysed process under UV-A irradiation, where hydroxyl radicals from photocatalytic TiO_2 reacted with Si–H bonds of PHPS. The formation of TiO_2@SiO_2 nanoparticles by this method exhibited a natural self-limiting behaviour, which guaranteed a consistent shell thickness independent of the PHPS concentration, thereby making the process more straightforward for large-scale industrial use compared to TEOS, which requires meticulous control of parameters. This approach offered superior control over photocatalytic passivation, achieving 89–96% passivation with TiO_2@PHPS nanoparticles and 88% with TiO_2/PHPS films, compared to only 30% passivation with traditional TEOS-derived SiO_2 shells. Additionally, PHPS did not compromise the whiteness of TiO_2@SiO_2 core–shell nanoparticles, essential for applications requiring pure white colours, while maintaining TiO_2's high-refractive-index optical properties and original colour characteristics in TiO_2/SiO_2 films. This demonstrates PHPS as a

superior alternative to TEOS for fabricating TiO_2@SiO_2 core–shell nanoparticles and films.

Author contributions

Darya Burak: conceptualization, investigation, data curation, formal analysis, writing – original draft, writing – review & editing. Jae Hyun Han: conceptualization, investigation, data curation, writing – original draft. Joon Soo Han: investigation, data curation, validation. In Soo Kim: investigation, writing – review & editing. Md Abdur Rahman: data curation, writing – review & editing. Joel K. W. Yang: validation, writing – review & editing. So-Hye Cho: conceptualization, validation, funding acquisition, project administration, resources, supervision, writing – review & editing.

Data availability

The data supporting this article have been included as part of the ESI.†

Conflicts of interest

The authors declare no conflicts of interest.

Acknowledgements

This research was supported by the Pioneer Research Center Program (RS-2024-00431320) and the Nano & Material Technology Development Program (2020M3H4A3106354) through the National Research Foundation of Korea funded by the Ministry of Education, Science and Technology.

References

1 X. Kang, S. Liu, Z. Dai, Y. He, X. Song and Z. Tan, *Catalysts*, 2019, **9**, 191.
2 H. R. Mohammed and D. M. H. Shinen, *Mater. Today: Proc.*, 2023, **81**, 459–463.
3 J. Molina-Reyes, A. Romero-Moran, H. Uribe-Vargas, B. Lopez-Ruiz, J. L. Sanchez-Salas, E. Ortega, A. Ponce, A. Morales-Sanchez, F. Lopez-Huerta and C. Zuñiga-Islas, *Catal. Today*, 2020, **341**, 2–12.
4 M. N. B. Razali, A. A. Alkaf and M. K. N. B. M. Zuhan, *Mater. Today: Proc.*, 2022, **48**, 1905–1909.
5 I. Nabi, A.-U. R. Bacha, F. Ahmad and L. Zhang, *J. Environ. Chem. Eng.*, 2021, **9**, 105964.
6 P.-J. Lu, S.-C. Huang, Y.-P. Chen, L.-C. Chiueh and D. Y.-C. Shih, *J. Food Drug Anal.*, 2015, **23**, 587–594.
7 R. J. B. Peters, G. van Bemmel, Z. Herrera-Rivera, H. P. F. G. Helsper, H. J. P. Marvin, S. Weigel, P. C. Tromp, A. G. Oomen, A. G. Rietveld and H. Bouwmeester, *J. Agric. Food Chem.*, 2014, **62**, 6285–6293.
8 F. W. Mont, J. K. Kim, M. F. Schubert, E. F. Schubert and R. W. Siegel, *J. Appl. Phys.*, 2008, **103**, 083120.
9 M. Bartoszewska, E. Adamska, A. Kowalska and B. Grobelna, *Molecules*, 2023, **28**, 645.
10 A. Vyatskikh, R. C. Ng, B. Edwards, R. M. Briggs and J. R. Greer, *Nano Lett.*, 2020, **20**, 3513–3520.
11 S. Ramesh, K. Govarthanan and A. Palaniappan, *Nanotoxicology*, 2023, **17**, 176–201.
12 H. W. Lim, I. Kohli, E. Ruvolo, L. Kolbe and I. H. Hamzavi, *J. Am. Acad. Dermatol.*, 2022, **86**, S27–S37.
13 W. Lyu, M. Qian and F. Yang, *Highl. Sci. Eng. Technol.*, 2022, **13**, 155–162.
14 J. Guo, D. Benz, T.-T. D. Nguyen, P.-H. Nguyen, T.-L. T. Le, H.-H. Nguyen, D. La Zara, B. Liang, H. T. Hintzen, J. R. van Ommen and H. V. Bui, *Appl. Surf. Sci.*, 2020, **530**, 147244.
15 I. A. Siddiquey, T. Furusawa, M. Sato, K. Honda and N. Suzuki, *Dyes Pigm.*, 2008, **76**, 754–759.
16 A. M. El-Toni, S. Yin, T. Sato, T. Ghannam, M. Al-Hoshan and M. Al-Salhi, *J. Alloys Compd.*, 2010, **508**, 1–4.
17 H. J. Kim, D. K. Roh, J. H. Chang and D.-S. Kim, *Ceram. Int.*, 2019, **45**, 16880–16885.
18 M. D. Purkayastha, T. P. Majumder, M. Sarkar and S. Ghosh, *Radiat. Phys. Chem.*, 2022, **192**, 109898.
19 O. K. Park, Y. S. Kang and B. G. Jo, *J. Ind. Eng. Chem.*, 2004, **10**, 733–738.
20 J.-W. Lee, S. Kong, W.-S. Kim and J. Kim, *Mater. Chem. Phys.*, 2007, **106**(1), 39–44.
21 E. Ukaji, K. Harigae, N. Suzuki, T. Furusawa and M. Sato, *Mater. Technol.*, 2006, **24**, 275–281.
22 H. Lee, S. Koo and J. Yoo, *J. Ceram. Process. Res.*, 2012, **13**, 300–303.
23 M. H. Lee, U. M. Patil, S. T. Kochuveedu, C. S. Lee and D. H. Kim, *Bull. Korean Chem. Soc.*, 2012, **33**, 3767.
24 H. J. Cha, O. K. Park, Y. H. Kim, H. G. Cha and Y. S. Kang, *Int. J. Nanosci.*, 2006, **5**, 795–801.
25 F. Bauer, U. Decker, A. Dierdoft, H. Ernst, R. Heller, H. Liebe and R. Mehnert, *Prog. Org. Coat.*, 2005, **53**, 183–190.
26 Y. Jeong, C. Pearson, H.-G. Kim, M.-Y. Park, H. Kim, L.-D. Do and M. C. Petty, *ACS Appl. Mater. Interfaces*, 2016, **8**, 2061–2070.
27 Z. Zhang, Z. Shao, Y. Luo, P. An, M. Zhang and C. Xu, *Polym. Int.*, 2015, **64**, 971–978.
28 H. Kozuka, K. Nakajima and H. Uchiyama, *ACS Appl. Mater. Interfaces*, 2013, **5**(17), 8329–8336.
29 V. Poliukhova, J.-K. Park, D. Kim, S. Khan, J. Y. Seo, S. J. Kim, G.-H. Moon, K.-Y. Baek, S. Kim and S.-H. Cho, *Chem. Eng. J. Adv.*, 2022, **12**, 100363.
30 Konica Minolta Sensing Inc., SpectraMagicTM NX Color Data Software. **https://sensing.konicaminolta.us/us/products/spectramagic-nx-color-data-software/**.
31 S. Larouche and L. Martinu, *Appl. Opt.*, 2008, **47**, 219–230.
32 K. Nakajima, H. Uchiyama, T. Kitano and H. Kozuka, *J. Am. Ceram. Soc.*, 2013, **96**(6), 2806–2816.

33 P. Magalhães, L. Andrade, O. C. Nunes and A. Mendes, *Rev. Adv. Mater. Sci.*, 2017, **51**, 91–129.
34 T. Furusawa, K. Honda, E. Ukaji, M. Sato and N. Suzuki, *Mater. Res. Bull.*, 2008, **43**, 946–957.
35 Y. Yu, Y. Zhu, J. Guo, H. Yue, H. Zhang, C. Liu, S. Tang and B. Liang, *Ind. Eng. Chem. Res.*, 2018, **57**, 8679–8688.
36 Y. Bai, Z. Li, B. Cheng, M. Zhang and K. Sua, *RSC Adv.*, 2017, **7**, 21758–21767.
37 Y. Lin, T. Wang and Y. Jin, *Powder Technol.*, 2002, **123**, 194–198.
38 G. Li, F. Liu and Z. Zhang, *J. Alloys Compd.*, 2010, **493**, L1–L7.
39 X. Wang, S. O. Pehkonen, J. Rämö, M. Väänänen, J. G. Highfield and K. Laasonen, *Catal. Sci. Technol.*, 2012, **2**, 784–793.
40 H. S. Lee, S. M. Koo and J. W. Yoo, *J. Ceram. Process. Res.*, 2013, **13**, 300–303.
41 E. Ukaji, T. Furusawa, M. Sato and N. Suzuki, *Appl. Surf. Sci.*, 2007, **254**, 563–569.
42 A. Kaur, P. Chahal and T. Hogan, *IEEE Electron Device Lett.*, 2016, **37**(2), 142–145.
43 T. Luttrell, S. Halpegamage, J. Tao, A. Kramer, E. Sutter and M. Batzill, *Sci. Rep.*, 2014, **4**, 4043.
44 G. Žerjav, K. Žižek, J. Zavašnik and A. Pintar, *J. Environ. Chem. Eng.*, 2022, **10**, 107722.
45 T. Han, H. Xue, X. Hu, R. Li, H. Liu and Y. Tu, *LWT–Food Sci. Technol.*, 2022, **159**, 113178.
46 X. Zhang, A. Fujishima, M. Jin, A. V. Emeline and T. Murakami, *J. Phys. Chem.*, 2006, **110**, 25142–22514.
47 R. S. Dubey, *Superlattices Microstruct.*, 2017, **111**, 1099–1103.
48 J. Wu, J. Tu, K. Hu, X. Xiao, L. Li, S. Yu, Y. Xie, H. Wu and Y. Yang, *Colloids Surf., A*, 2022, **654**, 130173.